Comparison of Standstill Parameter Identification Methods for Induction Motors

Sina Khamehchi, Eemeli Mölsä, and Marko Hinkkanen
Aalto University School of Electrical Engineering, Espoo, Finland

***Abstract*—This paper compares two different standstill identification schemes for the induction motor (IM) parameters. The schemes apply sinusoidal-excitation tests and DC-decay tests. Magnetic saturation of the motor is taken into account. The sensitivity of the parameter estimation to the stator resistance errors and the voltage errors is studied. Simulation results using a 2.2-kW IM drive are presented.**

***Index Terms*—Induction motor drives, parameter identification, saturation characteristics.**

I. Introduction

An induction machine (IM) is the most common machine in industrial applications. Various control methods are used to drive IMs, e.g., scalar control and rotor-flux-oriented vector control. Speed sensorless control schemes are often used in general-purpose drives. Control schemes require a knowledge of the motor equivalent circuit parameters and the performance of the controller relies on the accuracy of the motor parameters. These parameters are estimated by means of measurements during the drive initialization. Therefore, self-commissioning is needed as a starting phase for motor control.

Parameter identification has been studied widely and a great number of methods are available in literature. Some standstill identification schemes, e.g., [1], [2], do not take the magnetic saturation into account. The self-commissioning method in [3] is not a standstill procedure and also needs a speed sensor which is not available in standard drives. A detailed study on the dependency of the motor parameters on the operating points is carried out in [4]. However, this estimation scheme needs the motor to rotate. In [5], a standstill identification method has been proposed where a model reference adaptive system approach is used and a parallel adaptive observer is designed. The principle of the identification is based on preventing the occurrence of the saturation in the estimation process. To avoid the motor to enter the saturation, the rotor flux level estimator is used to check the state of the IM to be in the linear region. For the identification scheme, the adaptive reference model is needed which increases the complexity of the implementation.

An iterative identification method at standstill for the Γ model parameters introduced in [6]. This method is based on the single-axis sinusoidal excitation. In addition, a step-by-step method for the inverse-Γ model parameter estimation is presented in [7] and later improved in [8] where the DC-decay test and the DC-bias sinusoidal excitation are used.

In this paper, a detailed study on the properties of the identification schemes in [6] and [7] is conducted. These two methods are chosen for the comparison, since they are easily applicable and well-known both in academia and industry. In the identification procedure, the stator voltage is reconstructed by means of the DC-link voltage and switching duty cycles. Thus, the voltage distortion caused by the inverter produces an error in the stator voltage. Furthermore, the value of the stator resistance is not perfectly known, e.g., due to the temperature. The main contribution of this paper is the evaluation of the sensitivity of the methods to the stator resistance and stator voltage errors. Furthermore, the transformation for the estimated parameters of the inverse-Γ model to those of the Γ model is explained.

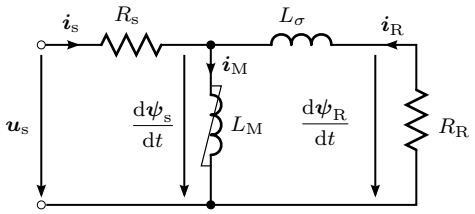

Fig. 1. Γ equivalent circuit at standstill.

II. Motor Model

For an appropriate comparison, the same motor model is used for both schemes. Hence, the dynamic Γ model at standstill is used as in Fig. 1. Complex space vectors are shown in boldface. The voltage equations at standstill in the stationary reference frame are given as

$$\frac{\mathrm{d}\boldsymbol{\psi}_\mathrm{s}}{\mathrm{d}t} = \boldsymbol{u}_\mathrm{s} - R_\mathrm{s}\boldsymbol{i}_\mathrm{s} \tag{1a}$$

$$\frac{\mathrm{d}\boldsymbol{\psi}_\mathrm{R}}{\mathrm{d}t} = -R_\mathrm{R}\boldsymbol{i}_\mathrm{R} \tag{1b}$$

where $\boldsymbol{u}_\mathrm{s}$ is the stator voltage, R_s is the stator resistance, R_R is the rotor resistance, $\boldsymbol{i}_\mathrm{s}$ is the stator current, $\boldsymbol{i}_\mathrm{R}$ is the rotor current, $\boldsymbol{\psi}_\mathrm{s}$ is the stator flux, and $\boldsymbol{\psi}_\mathrm{R}$ is the rotor flux.

Inductances of the motor depend on the magnetic state and vary in different operating points. In the rated operating point, IMs are saturated magnetically due to their design for producing maximum torque. The magnetic saturation should be taken into account when, e.g., the field-weakening or loss-minimizing flux level control is needed [9]. In the field-weakening region where the stator flux decreases, the stator inductance increases. In the Γ model, the magnetizing inductance L_M can be modeled as a function of the stator flux and the leakage inductance L_σ is often assumed constant [9].

978-1-5386-4455-3/18/$31.00 ©2018 IEEE

Various mathematical models for the saturation characteristics can be found in literature. A rational function is used here as [9], [10]

$$L_{\mathrm{M}}(\psi_{\mathrm{s}}) = \frac{1}{c_0 + c_{\mathrm{s}}\psi_{\mathrm{s}}^S} \tag{2}$$

where c_0 is the inverse of the unsaturated inductance, c_{s} is a positive coefficient, S is a positive exponent and $\psi_{\mathrm{s}} = |\boldsymbol{\psi}_{\mathrm{s}}|$ is the stator flux magnitude. Exponent S determines the shape of the saturation curve and is normally in the range of $5 \leq S \leq 9$ [6]. The hysteresis and eddy-current losses as well as the deep-bar effect of the motor are omitted.

III. Identification Methods

A. Single-Axis Sinusoidal Excitation

The excitation signal of the method in [6] is the sinusoidal current along one axis as

$$\boldsymbol{i}_{\mathrm{s}} = I_{\mathrm{s}} \sin \omega t \tag{3}$$

The magnetizing inductance is identified using a lower angular frequency

$$\omega \approx \frac{1}{8}\frac{R_{\mathrm{R}}}{L_\sigma} \tag{4}$$

and the leakage inductance is identified using a higher angular frequency

$$\omega \approx \frac{1}{2}\frac{R_{\mathrm{R}}}{L_\sigma} \tag{5}$$

To create different operating points, a set of current amplitudes I_{s} is chosen within a range of zero to the nominal current of the motor. The sinusoidal currents with two angular frequencies given in (4) and (5) are fed to the motor and the stator voltage and current phasors are calculated.

Knowing one of the inductances in a certain operating point, the other inductance and the rotor resistance can be obtained by means of the measured data for the same operating point. Therefore, all Γ model parameters can be calculated iteratively by means of the steady-state equations. The iteration at each point starts with an initial guess for the leakage inductance $L_\sigma(0)$ since one of the inductances should be known. Using $L_\sigma(0)$, the magnetizing inductance and the rotor resistance are calculated by means of the phasors achieved from the lower frequency test data. The calculated rotor resistance and magnetizing inductance are used to obtain the leakage inductance using the higher frequency test data for the same operating point. The iteration at each operating point continues till the leakage inductance converges to a fixed value. The iterative procedure is repeated for all of the chosen operating points.

In the beginning of the identification, the leakage inductance is unknown. Therefore, the initial guess of the leakage inductance $L_\sigma(0)$ contains some errors inevitably. Fig. 2 illustrates the robustness of the method against the initial guess of the leakage inductance. The initial guess for the leakage inductance can be in the range of zero to approximately five times of the actual L_σ value. In addition, simulations show that the convergence of L_σ takes only a few number of iteration cycles (around four cycles).

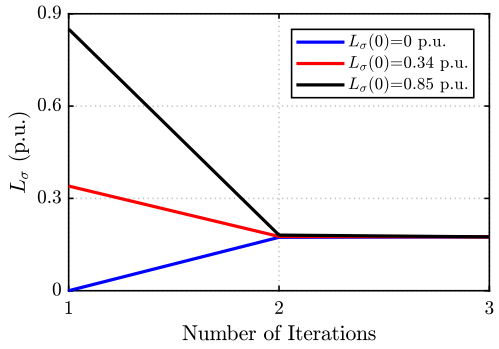

Fig. 2. Convergence of the leakage inductance estimate as a function of the iteration cycles.

B. DC-Decay Test and DC-Biased Sinusoidal Excitation

The identification method in [7] consists of different steps. The magnetizing inductance is identified by the DC-decay test, feeding the motor with the DC current in order to create a DC steady-state operating point. Thereafter, the stator terminals are short-circuited using a zero voltage vector and the flux is estimated using the voltage model until the steady state is reached. The magnetizing inductance at each operating point is obtained by dividing the estimated stator flux in the steady state by the DC current magnitude $i_{\mathrm{s,dc}}$ as

$$L_{\mathrm{M}} = -\frac{1}{i_{\mathrm{s,dc}}} \lim_{t\to\infty} \int_0^t (\boldsymbol{u}_{\mathrm{s}} - R_{\mathrm{s}}\boldsymbol{i}_{\mathrm{s}})\mathrm{d}t \tag{6}$$

The leakage inductance is identified using a DC-biased sinusoidal voltage as

$$\boldsymbol{u}_{\mathrm{s}} = U_{\mathrm{s0}} + U_{\mathrm{s}} \sin \omega t \tag{7}$$

where a sinusoidal signal with a small amplitude U_{s} is superimposed to a set of DC-bias voltages U_{s0}. This signal produces a sinusoidal current as

$$\boldsymbol{i}_{\mathrm{s}} = I_{\mathrm{s0}} + I_{\mathrm{s}} \sin(\omega t + \phi) \tag{8}$$

lagging the voltage by the angle ϕ. The DC-bias voltages are chosen to produce the DC currents within the range of zero to the nominal rating of the motor. The frequency for identification of the leakage inductance can be about five times the rated frequency.

The rotor resistance is identified using a DC-biased sinusoidal voltage with a single DC offset. This DC offset should be high enough to move the AC voltage from the near-zero region due to inverter nonlinearity. The frequency for estimating the rotor resistance can be within a range from zero to the nominal slip frequency. The Goertzel algorithm can be used to compute the phasors in a computationally efficient way [7].

IV. Model Transformation

The inverse-Γ model parameters are estimated in [7] while the Γ model parameters are identified in [6]. For a proper comparison, the estimated parameters of both schemes should be for the same model. In this paper, the Γ model is preferred

as the reference since, e.g., the leakage inductances of the T model cannot be identified uniquely, and this model is not adequate for a saturated IM [11]. Additionally, modelling the saturation may become simpler in the Γ model as compared to the inverse-Γ model [9]. The parameters of the inverse-Γ model can be transformed into those of the Γ model and vice versa by means of the scaling factor [11]. If the Γ model is assumed, the scaling factor can be calculated as

$$\gamma = \frac{L_\mathrm{M}}{L_\mathrm{M} + L_\sigma} \tag{9}$$

and the inverse-Γ parameters are obtained using the scaling factor as

$$L'_\sigma = \gamma L_\sigma \qquad R'_\mathrm{R} = \gamma^2 R_\mathrm{R} \tag{10}$$

This transformation can also be used when the incremental inductances are considered [12]. First, the chord-slope magnetizing inductance L_M is identified by the DC-decay test. In the saturation model (2), the exponent S can be fixed and the coefficients c_0 and c_s can be estimated directly by means of the linear least squares (LLS) method [13]. In the second step, the incremental inverse-Γ leakage inductance $L'_{\sigma\mathrm{i}}$ is identified using a set of DC voltages superimposed to a high-frequency AC signal. According to Fig. 1, the DC component and a part of the sinusoidal current flows through the magnetizing branch. This sinusoidal current component sees the incremental inductance L_Mi, whose value can be obtained by inserting the estimated c_0 and c_s into

$$L_\mathrm{Mi}(\psi_\mathrm{s}) = \frac{1}{c_0 + (S+1)c_\mathrm{s}\psi_\mathrm{s}^S} \tag{11}$$

Inserting (9) into (10) leads to

$$L'_{\sigma\mathrm{i}} = \frac{L_\mathrm{Mi}}{L_\mathrm{Mi} + L_{\sigma\mathrm{i}}} L_{\sigma\mathrm{i}} \tag{12}$$

from which the Γ model leakage inductance becomes

$$L_{\sigma\mathrm{i}} = \frac{L_\mathrm{Mi}}{L_\mathrm{Mi} - L'_{\sigma\mathrm{i}}} L'_{\sigma\mathrm{i}} \tag{13}$$

Therefore, the scaling factor γ_i is calculated as

$$\gamma_\mathrm{i} = \frac{L_\mathrm{Mi} - L'_{\sigma\mathrm{i}}}{L_\mathrm{Mi}} \tag{14}$$

and the Γ model leakage inductance $L_{\sigma\mathrm{i}}$ and rotor resistance R_R are obtained using the scaling factor as

$$L_{\sigma\mathrm{i}} = \frac{L'_{\sigma\mathrm{i}}}{\gamma_\mathrm{i}} \qquad R_\mathrm{R} = \frac{R'_\mathrm{R}}{\gamma_\mathrm{i}^2} \tag{15}$$

It is worth mentioning that $L_\sigma = L_{\sigma\mathrm{i}}$ since it is assumed constant here.

V. Simulation Results

Identification methods in [6] and [7] have been implemented using a 2.2-kW induction motor with the rating given in Table I. The estimation errors are evaluated and simulation results are provided in the following.

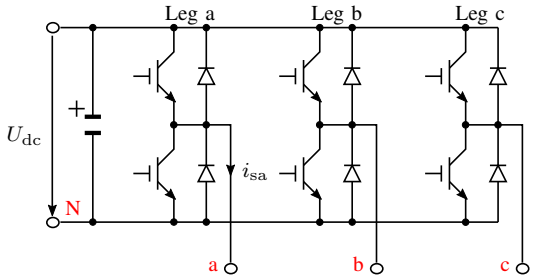

Fig. 3. Schematics of a three-phase inverter.

TABLE I
Rating of 2.2-kW Four-Pole IM

Power P_N	2.2 kW
Voltage U_N	400 V
Frequency f_N	50 Hz
Current I_N	5 A
Speed n_N	1430 r/min

A. Sources of Error

Two main sources of inaccuracy in the IM parameter identification can be considered as the stator resistance estimation error and voltage error caused by the inverter. The effect of the mentioned errors on the estimation results cannot be separated in practice. Nonetheless, by separating the sources of error in simulations, the effect of each one can be evaluated. The effect of the stator resistance error on other parameters is evaluated by considering $\hat{R}_\mathrm{s} = 0.9R_\mathrm{s}$ and $\hat{R}_\mathrm{s} = 1.1R_\mathrm{s}$, where $\hat{R}_\mathrm{s}$ is the resistance estimate.

Fig. 3 shows a three-phase inverter schematics. Inverter nonlinear characteristics are mainly due to the dead time and the voltage drop caused by the switches and diodes when conducting [14]. These nonlinear characteristics produce an error between the reference voltage and the inverter output voltage. The stator voltage error can be evaluated separately. For this purpose, the actual stator voltage u_sa for the phase a is defined according to (and similarly for other phases)

$$u_\mathrm{sa} = u_\mathrm{sa,ref} - u_\mathrm{err}\,\mathrm{sign}(i_\mathrm{sa}) \tag{16}$$

where $u_\mathrm{sa,ref}$ is the reference phase voltage and u_err is the constant voltage error [14]. The constant voltage error can be defined as

$$u_\mathrm{err} = \frac{T_\mathrm{d}}{T_\mathrm{s}} U_\mathrm{dc} + u_\mathrm{th} \tag{17}$$

where T_d is the switching dead time, U_dc is the DC-link voltage, and u_th is the threshold voltage of the switch. The on-state resistances of the switches are omitted, since the stator resistance estimation includes all the resistive components of the inverter. The considered values for the voltage error u_err are 0.0006 p.u. (0.2 V) and 0.0012 p.u. (0.4 V). An accurate stator resistance estimate, $\hat{R}_\mathrm{s} = R_\mathrm{s}$, is assumed.

B. Magnetizing Inductance

Figs. 4 and 5 show the estimation of L_M in ideal conditions using the single-axis sinusoidal excitation and the DC-decay

test, respectively. Estimation is accurate in both schemes while the motor is not saturated. However, when the magnetizing inductance starts to saturate, an error occurs with the single-axis sinusoidal excitation. This phenomenon has been studied in [15]. Firstly, the chord-slope inductance L_{M} is pulsating in the single-phase sinusoidal excitation while it is constant in the three-phase excitation. Increasing the excitation current amplitude increases the fluctuation in L_{M}. The deeper the saturation level, the larger the error in the magnetizing inductance estimate becomes. Fig. 6 shows the magnetizing inductance in the single-phase and three-phase excitations, and the estimate of L_{M} when the motor is highly saturated. Fig. 7 illustrates the fluctuation of the flux as a function of the magnetizing current in a highly saturated region where the hysteresis loop is omitted for simplicity. The stator flux pulsates between two points, 1 and 2, which is shown with red color. This pulsating area contains the linear region and saturation region. In the linear region, the chord-slope L_{M} and incremental L_{Mi} are equal. In the saturation region, the incremental inductance changes due to the change in the tangent of the saturation curve. In this region, the higher is the saturation, the higher is the amplitude of the fluctuation of the chord-slope inductance L_{M}. However, the incremental inductance L_{Mi} decreases due to the decrease in the tangent of the saturation curve. The effect of the incremental inductance varies with the excitation current amplitude and the error becomes larger with the rise in the current amplitude.

Fig. 4 illustrates the estimated magnetizing inductance, taking the stator resistance errors into account. The DC-decay test is less sensitive to the stator resistance errors. Fig. 5 shows the sensitivity of the identification methods to the stator voltage errors. It can be seen that both methods are very sensitive to the stator voltage errors.

C. Leakage Inductance

The leakage inductance is estimated using the single-axis and DC-biased sinusoidal excitation methods. Results show an estimation error around 1%. Hence, both methods estimate the leakage inductance accurately in ideal conditions. Fig. 8(a) illustrates the estimation errors of L_σ obtained by the DC-biased sinusoidal excitation. It can be concluded that the estimation errors of the leakage inductance L_σ are low in both schemes.

In the presence of the inverter voltage errors, the estimation errors of L_σ using single-axis sinusoidal signal is quite low and negligible. Fig. 8(b) illustrates the estimated L_σ using DC-biased sinusoidal excitation in the presence of the voltage errors. In this case, the single-axis sinusoidal excitation is robust against the inverter voltage errors. It can be concluded from the expression (14) that in the presence of the voltage errors, the estimation errors in L_σ using DC-biased voltage is caused by the magnetizing inductance error since the estimated inverse-Γ leakage inductance is robust against the voltage errors. Fig. 9 shows the robustness of the inverse-Γ leakage inductance L'_σ against the stator voltage errors.

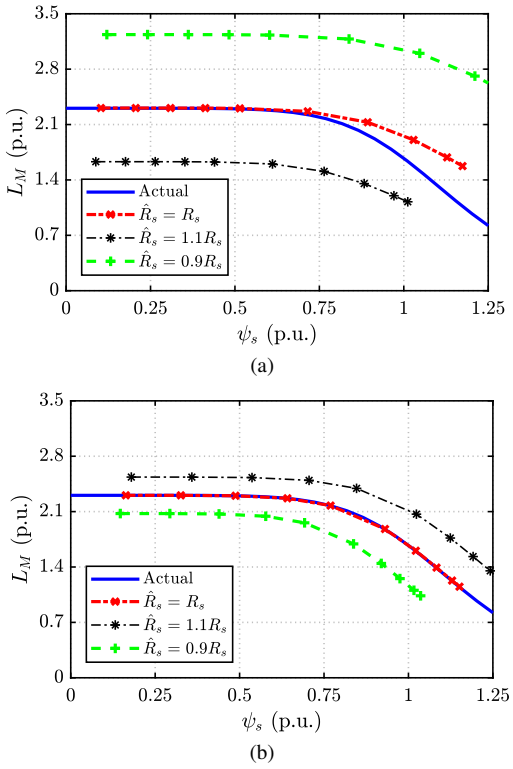

Fig. 4. Simulation results of L_{M} identification including R_{s} errors: (a) single-axis sinusoidal excitation; (b) DC-decay test.

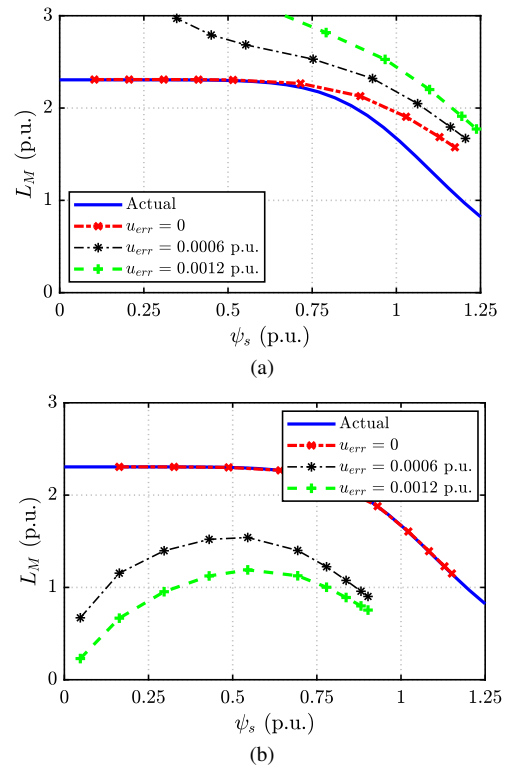

Fig. 5. Simulation results of L_{M} identification including voltage errors: (a) single-axis sinusoidal excitation; (b) DC-decay test.

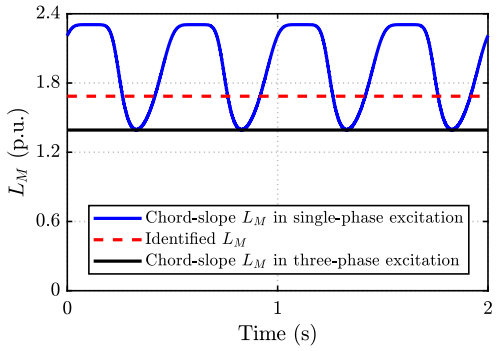

Fig. 6. Chord-slope magnetizing inductance in the single-phase and three-phase excitations, with its estimated value using the method in [6], when the motor is highly saturated.

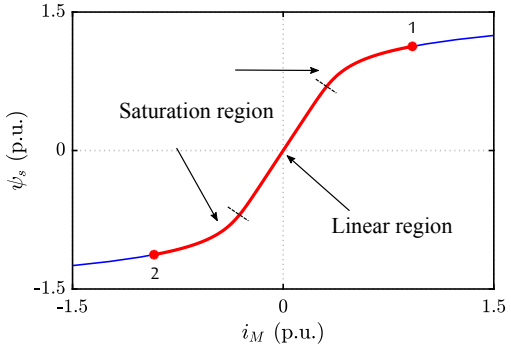

Fig. 7. Graphical interpretation of the pulsating stator flux as a function of the magnetizing current in the single-phase excitation when the motor is highly saturated.

D. Rotor Resistance

The rotor resistance is estimated using single-axis and DC-biased sinusoidal signals. In ideal conditions, both schemes show a high accuracy and the estimation error is around 1% for both methods. By adding the stator resistance errors, the estimated rotor resistance using the single-axis sinusoidal signal has an error around 12%. However, the estimation error using the DC-biased sinusoidal excitation varies when different DC offset currents are used. Simulations show lower errors when the DC offset current of around 0.5 p.u. is used. In case of the voltage error effects on the estimated R_{R}, the method based on the single-axis sinusoidal signal is relatively robust. This error is low as compared to the error in the case of the DC-biased sinusoidal excitation.

VI. Conclusions

The properties of the two standstill identification methods are compared. The methods are based on the single-axis and DC-biased sinusoidal excitation signals in addition to the DC-decay test. The estimation of the magnetizing inductance becomes inaccurate in the saturated region in the case of the single-axis sinusoidal excitation due to the incremental inductance effect. On the contrary, the DC-decay test is a more suitable method for the magnetizing inductance identification. In addition, the DC-decay test is more robust against the stator resistance errors as compared to the single-axis sinusoidal excitation. The estimation errors of the leakage inductance are low in both methods when the stator resistance errors are taken into account. Both methods are highly sensitive to the inverter voltage errors in the case of the magnetizing inductance estimation. However, the iterative method based on the single-axis sinusoidal excitation can tolerate these errors better in the case of the leakage inductance and rotor resistance identification. The estimation accuracy of the rotor resistance using the DC-biased excitation, in the presence of errors, including the stator resistance errors and voltage errors, depends on the DC offset current.

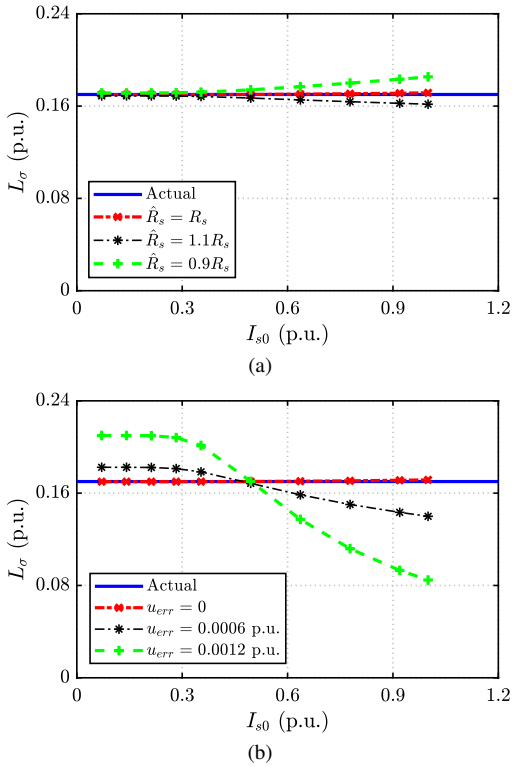

Fig. 8. Simulation results of L_σ identification using the DC-biased sinusoidal excitation in the presence of: (a) stator resistance estimation errors; (b) stator voltage errors.

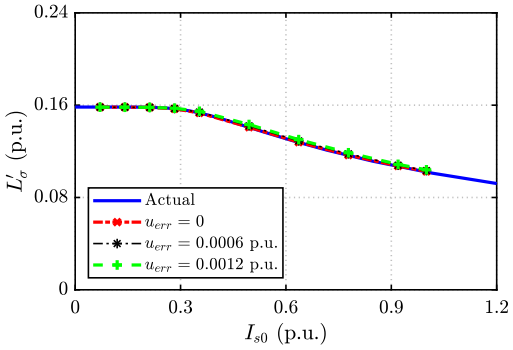

Fig. 9. Robustness of L'_σ identification against stator voltage errors.

REFERENCES

[1] L. Monjo, H. Kojooyan-Jafari, F. Córcoles, and J. Pedra, "Squirrel-cage induction motor parameter estimation using a variable frequency test," *IEEE Trans. Energy Convers.*, vol. 30, no. 2, pp. 550–557, June 2015.

[2] S. H. Lee, A. Yoo, H. J. Lee, Y. D. Yoon, and B. M. Han, "Identification of induction motor parameters at standstill based on integral calculation," *IEEE Trans. Ind. Appl.*, vol. 53, no. 3, pp. 2130–2139, May 2017.

[3] A. M. Khambadkone and J. Holtz, "Vector-controlled induction motor drive with a self-commissioning scheme," *IEEE Trans. Ind. Electron.*, vol. 38, no. 5, pp. 322–327, Oct. 1991.

[4] A. B. Proca and A. Keyhani, "Identification of variable frequency induction motor models from operating data," *IEEE Trans. Energy Convers.*, vol. 17, no. 1, pp. 24–31, Mar. 2002.

[5] P. Castaldi and A. Tilli, "Parameter estimation of induction motor at standstill with magnetic flux monitoring," *IEEE Trans. Control Syst. Technol.*, vol. 13, no. 3, pp. 386–400, May 2005.

[6] N. R. Klaes, "Parameter identification of an induction machine with regard to dependencies on saturation," *IEEE Trans. Ind. Appl.*, vol. 29, no. 6, pp. 1135–1140, Nov. 1993.

[7] L. Peretti and M. Zigliotto, "Automatic procedure for induction motor parameter estimation at standstill," *IET Electr. Power Appl.*, vol. 6, no. 4, pp. 214–224, Apr. 2012.

[8] M. Carraro and M. Zigliotto, "Automatic parameter identification of inverter-fed induction motors at standstill," *IEEE Trans. Ind. Electron.*, vol. 61, no. 9, pp. 4605–4613, Sep. 2014.

[9] Z. Qu, M. Ranta, M. Hinkkanen, and J. Luomi, "Loss-minimizing flux level control of induction motor drives," *IEEE Trans. Ind. Appl.*, vol. 48, no. 3, pp. 952–961, May 2012.

[10] H. C. J. de Jong, "Saturation in electrical machines," in *Proc. International Conference on Electrical Machines*, vol. 3, Athens, Greece, Sep. 1980, pp. 1545–1552.

[11] G. R. Slemon, "Modelling of induction machines for electric drives," *IEEE Trans. Ind. Appl.*, vol. 25, no. 6, pp. 1126–1131, Nov. 1989.

[12] J. Godbersen, "A stand-still method for estimating the rotor resistance of induction motors," in *Conf. Rec. IEEE Ind. Appl. Annu. Meeting*, vol. 2, Oct 1999, pp. 900–905.

[13] M. Hinkkanen, P. Pescetto, E. Mölsä, S. E. Saarakkala, G. Pellegrino, and R. Bojoi, "Sensorless self-commissioning of synchronous reluctance motors at standstill without rotor locking," *IEEE Trans. Ind. Appl.*, vol. 53, no. 3, pp. 2120–2129, May 2017.

[14] J.-W. Choi and S.-K. Sul, "Inverter output voltage synthesis using novel dead time compensation," *IEEE Trans. Power Electron.*, vol. 11, no. 2, pp. 221–227, Mar 1996.

[15] J. Y. Ruan and S. M. Wang, "Magnetizing curve estimation of induction motors in single-phase magnetization mode considering differential inductance effect," *IEEE Trans. Power Electron.*, vol. 31, no. 1, pp. 497–506, Jan. 2016.